ISSN: 2832-7705

Review Article

International Journal of Clinical and Medical Education Research

Reconstruction of Cardiac Images using the Confocal Laser Scanning Microscope

Abdallah Hamed[1*] and T Al-Saeed[2]

[1]*Physics Dept., Fac. Sci., Ain shams University 11566 Cairo, Egypt*

[2]*Biomedical Department, Fac. Engineering, Helwan University, Cairo, Egypt*

[*]Corresponding Author
Abdallah Hamed , Physics Dept., Fac. Sci., Ain shams University 11566 Cairo, Egypt.

Submitted: 2023, Sep 08; **Accepted**: 2023, Oct 13; **Published**: 2023, Nov 15

Citation: Hamed, A., Saeed, A.T., (2023), Reconstruction of Cardiac Images Using the Confocal Laser Scanning Microscope. *Int J Clin Med Edu Res, 2*(11), 323-337.

Abstract

We suggested a cardioid aperture in the processing of cardiac images using the confocal laser scanning microscope (CSLM). We calculated the Point Spread Function (PSF) corresponding to the cardioid aperture and the cardiac images by using the FFT algorithm. Then, we studied the effect of the image rotation on the PSF. In addition, we computed the autocorrelation corresponding to the cardiac images and cardiac aperture and compared them with the autocorrelation of the uniform circular aperture. Also, we computed the cross-correlation of aligned and rotated cardiac images. Finally, we imaged the cardiac images using the confocal scanning microscope provided with the circular and cardioid shapes of apertures. The MATLAB code is used in the formation of all images and plots.

Keywords: Cardiac Images and Cardiac Apertures, Confocal Laser Scanning Microscope, The Point Spread Function of Cardiac Aperture, Coherent Transfer Function.

1. Introduction

Digital Image processing is the art of treatment of digital images to enable getting information from the image [1]. The first research comes from the science of astronomy regarding stars and galaxies. These images give results for medical imaging which is a major concern of in vivo diagnosis instead of in vitro. Imaging diseased organs can give rise to a diagnosis without applying a biopsy [2]. Biopsy hurts on the other side imaging is quite easy and simple. The digital image is presented as an image where the intensity in the image is quantized in 256 × 512 gray levels. On the other hand, color images can be discussed. The digital image is used treated by algebraic and mathematical tools to obtain different information about the image. For example, digital differentiation can result in edge detection and the skeleton of objects in the image. Spatial and frequency filters can apply to an image to get the edged image or get the averaged image by low-frequency pass. Fourier transforms (FT) are computed using MATLAB, or it is imaged in space by a convex length. We can pass or reject different regions of frequency of interest. Moreover, the morphological operation was found to provide different image manipulations to provide the necessary image processing techniques [3]. Different algorithms are applied to the image [4-5]. Moreover, random processes faced in images and signal processing are random. Thus, the image is random. Processing images requires image random processing or using a fuzzy technique [6-7]. It is known that the confocal scanning laser microscope consists of two objectives arranged in tandem where the scanned object is placed in the common short focus corresponding to the two objectives as shown in Figure (1). The image is shown in the detection plane constructed where the electronic scanning is synchronized with the mechanical scanning of the object. This confocal microscope considers coherent illumination emitted from the laser beam and coherent detection. Consequently, the intensity corresponding to the image is the modulus square of the convolution product of the object and the resultant PSF. The resultant PSF is the simple product of the PSF corresponding to the two apertures. In this study, one aperture is of cardiac shape while the other aperture has a uniform circular shape.

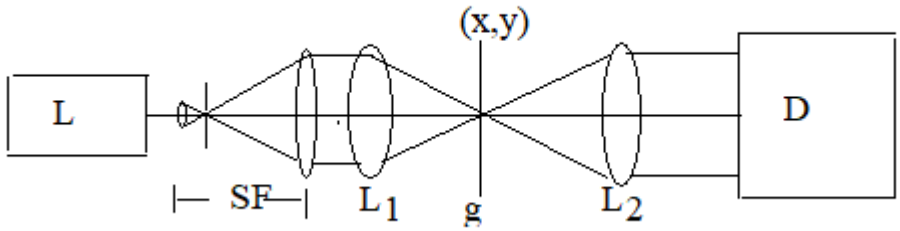

Recently, image processing of medical images based on speckle imaging technique and its contrast presented in while the image processing using the confocal scanning laser microscope provided with modulated apertures outlined in [8-15]. Another recent work using the confocal microscope was presented in Compressive light-field microscopy for 3-D neural activity recording is shown in [16]. A remodeling of cardiac tissue was analyzed, and a comprehensive approach based on confocal microscopy leading to 3D reconstruction was presented in [17]. Catheterized Fiber-Optics Confocal Microscopy of the Beating Heart in Situ was investigated in [18]. The aim of this work is the processing of the cardiac image using a cardiac aperture in the confocal scanning laser microscope. The paper is organized as follows. The second section presents an analysis of the computation of the Point Spread Function (PSF) using a cardioid curve. Section 3 presents the results and discussion. Section 4 presents conclusions.

2. Analysis

The cardiac aperture in cartesian coordinates is represented as follows [1,2]:

$$p(x,y) = 1; \frac{(x^2+y^2-2ax)^2}{4a(x^2+y^2)} \leq 1$$

$$= 0; \text{otherwise.} \quad (1)$$

In polar coordinates, it is represented as follows:

$$p(\rho,\theta) = 1;\ \rho(\theta) = 2a[1-\cos(\theta)] \quad (2)$$

a is a constant, while the radius ρ changed with the angle q.
The constant a deduced from equation (1) as follows:

$$a = \frac{x^2+y^2}{2[x+\sqrt{x^2+y^2}]} \quad (3)$$

Eq (3) only holds for these variables (x) and (y) which lie on the contour of the cardioid and of course not for any (x), (y) as suggested by eq 3.
The parametric equations of planar cardioid are written as follows:

$$x = 2\,a\cos(\theta)\ [1-\cos(\theta)]\,,\ and\ y = 2\,a\sin(\theta)\ [1-\cos(\theta)] \quad (4)$$

The PSF for the cardiac aperture is computed by applying the Fourier transform in polar coordinates as follows:

$$h(r) = \int_0^{2\pi}\int_0^{\rho} P(\rho,\theta)\exp\{-\frac{j2\pi}{\lambda f}(\rho r\cos\theta)\}\ \rho\, d\rho\, d\theta \quad (5)$$

where ρ is a variable dependent on the angle θ, represented by equation (2), and r is the radial coordinate in the Fourier plane where $r = \sqrt{u^2+v^2}$.

In the next section, we computed the PSF corresponding to the cardiac aperture Equation (2) using the fast Fourier transform (FFT).

3. Results and Discussions

We computed the cardiac aperture from Equation (1) and Equation (2), using MATLAB code, and plotted it as in Fig. (2). The radius ρ is not a constant like in circular aperture, it varied, according to Equation (2), in the range [0, 2]. The cardioid aperture shown in the L.H.S. Cardioid aperture is assumed as a model for comparison with the heart image shown in the R.H.S. as in Fig. (2). The two images have dimensions of 1024×1024 pixels. The average radius for the aperture is 128 pixels while, for the heart image, the average radius is 256 pixels. The cardioid aperture image was constructed using the formula for the cardioid curve [1]. The heart image rotation from θ = [0^0 180^0], where θ = 15^0 shown in Fig.

(3) while other image rotations are evident. The normalized PSF corresponding to the aperture of cardioid shape, using the FFT at maximum radius = 32 pixels, is computed and plotted as shown in figure (4- a). From the curve, it shows that the FWHM = 15 pixels. While it is computed for the cardiac image and plotted as shown in Figure (4- b). A comparative plot for the normalized PSF for a circular aperture of radius = 32 pixels is shown in Figure (4- c). The FWHM is shown as equal to 20 pixels. It shows that the heart image PSF is narrower compared with the PSF corresponding to the cardiac and circular apertures. In addition, the PSF has an asymmetric distribution which is attributed to the heart geometry compared with the symmetric shapes for the cardiac and circular apertures. It shows the stronger legs in figures (4 a, c) compared with the weaker legs in figures (4- b) correspond to the PSF plot of the heart image. Hence, the resolution attained for the heart image is better than the resolution obtained in the case of cardiac and circular apertures. Comparing the PSF corresponding to the circular and cardioid apertures we get a narrower FWHM for the cardioid aperture compared with the FWHM for the circular aperture as shown in the figures (4 a, c).

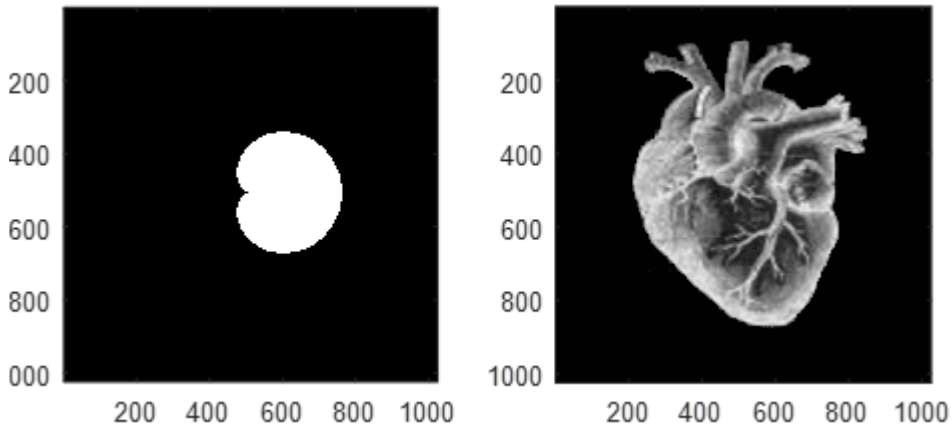

Figure 2: In the L.H.S. Cardioid aperture is shown while in the R.H.S., the heart image is shown. The two images have dimensions of 1024×1024 pixels. The maximum radius for the aperture = 256 pixels while the max. radius for the heart image = 512 pixels.

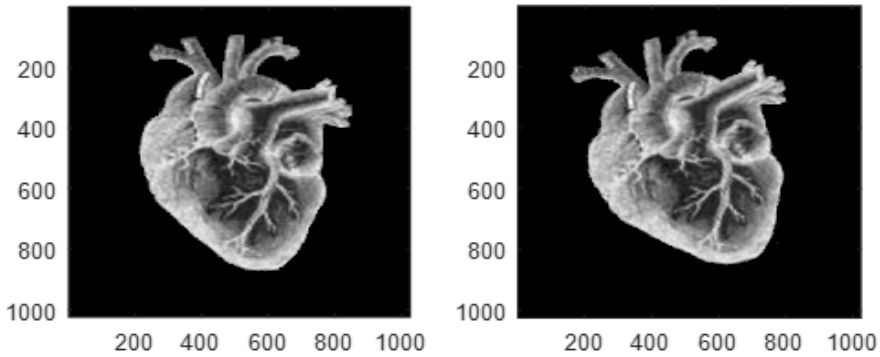

Figure 3: In the L.H.S. heart image is aligned along the cartesian coordinates shown while in the R.H.S., the heart image is inclined with an angle θ = 150 shown.

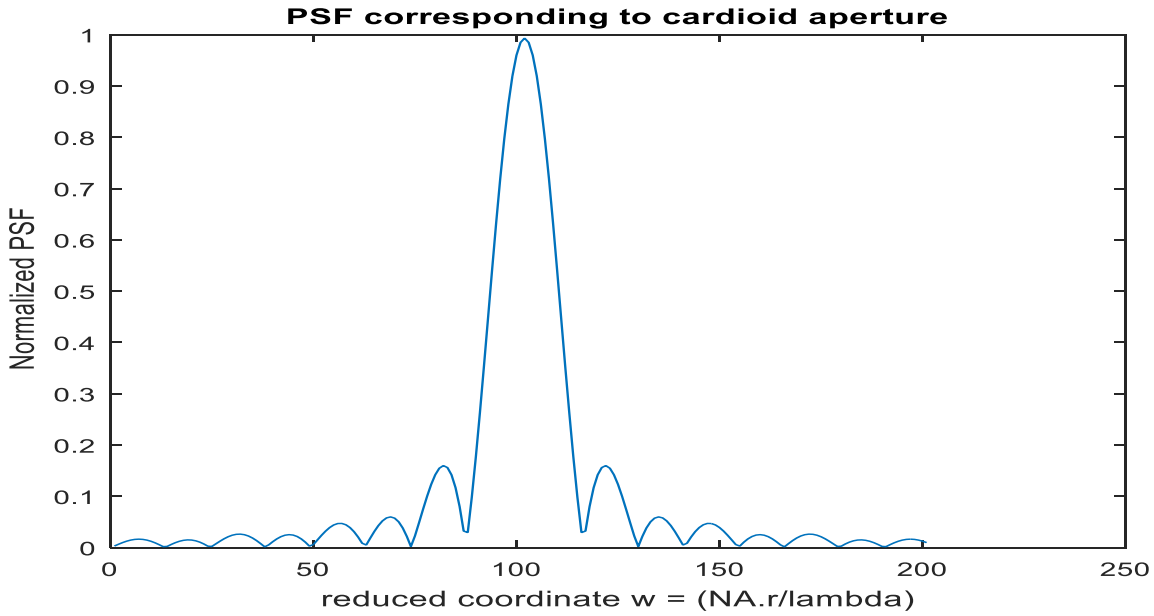

Figure 4- a: Normalized PSF corresponding to the aperture of the cardioid shape of maximum radius = 32 pixels. The FWHM is shown as equal to 15 pixels.

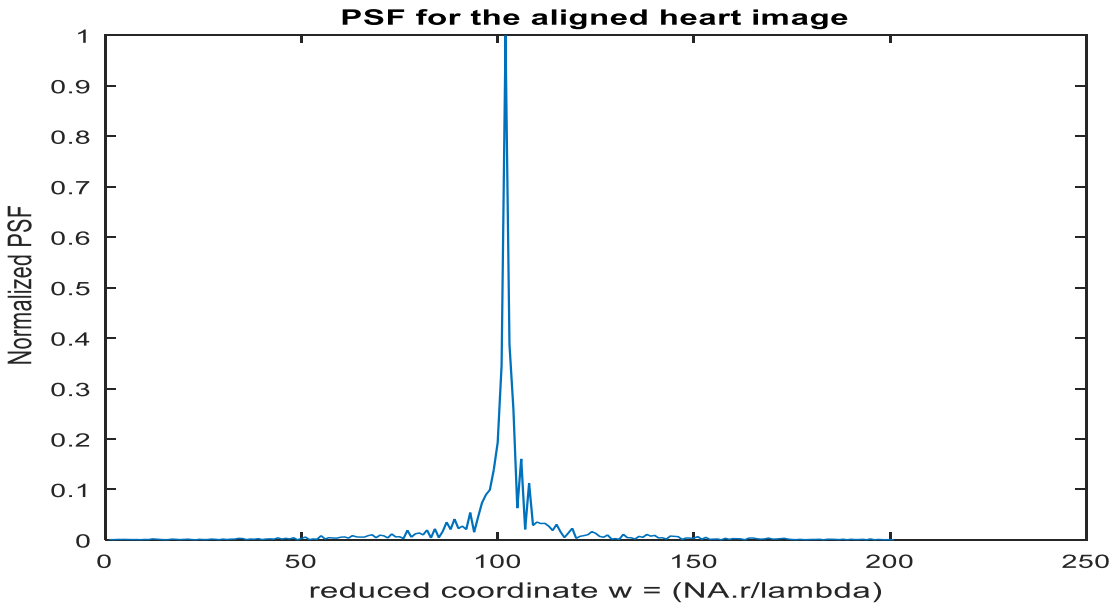

Figure 4-b: Normalized PSF corresponding to the cardiac image. The FWHM has an asymmetric distribution which is attributed to heart geometry.

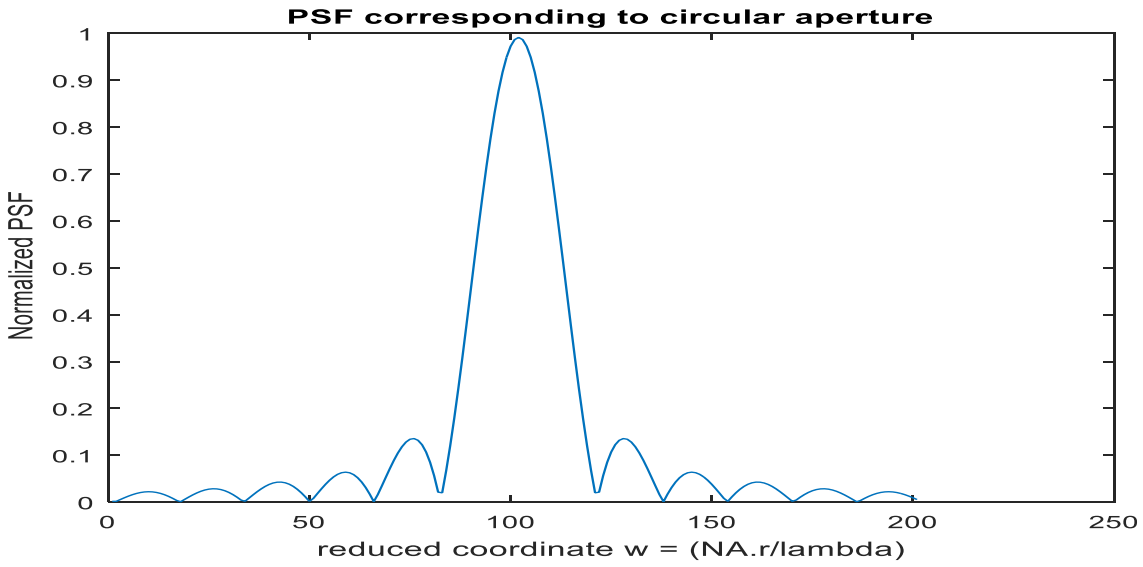

Figure 4- c: Normalized PSF for a circular aperture of radius = 32 pixels. The FWHM is shown as equal to 20 pixels.

The PSF corresponds to the rotated images computed and plotted as shown in the figure (5: a, b, …). It shows the asymmetric distribution for the PSF corresponding to image rotation. In addition, the PSF is sensitive to image rotation since the shape modified in the PSF ranges from 0 up to 0.3 around the peak. It is interesting to show the same profile for the PSF for the unrotated image shown in Figure (4-b) and its rotated image with $\theta = 180^0$ shown in Figure (5-a). The autocorrelation function of the aperture of cardioid shape was computed and plotted as shown in Figure (6). A line plot corresponding to the autocorrelation of the cardioid model at y = 512 pixels is shown in Figure (7-a). The calculated FWHM = 81 pixels. While the line plot at x = 512 pixels is shown in Figure (7-b). The FWHM = 68 pixels. Hence, unequal values of FWHM are shown attributed to the elongation of the cardioid aperture along one of the axes to the other.

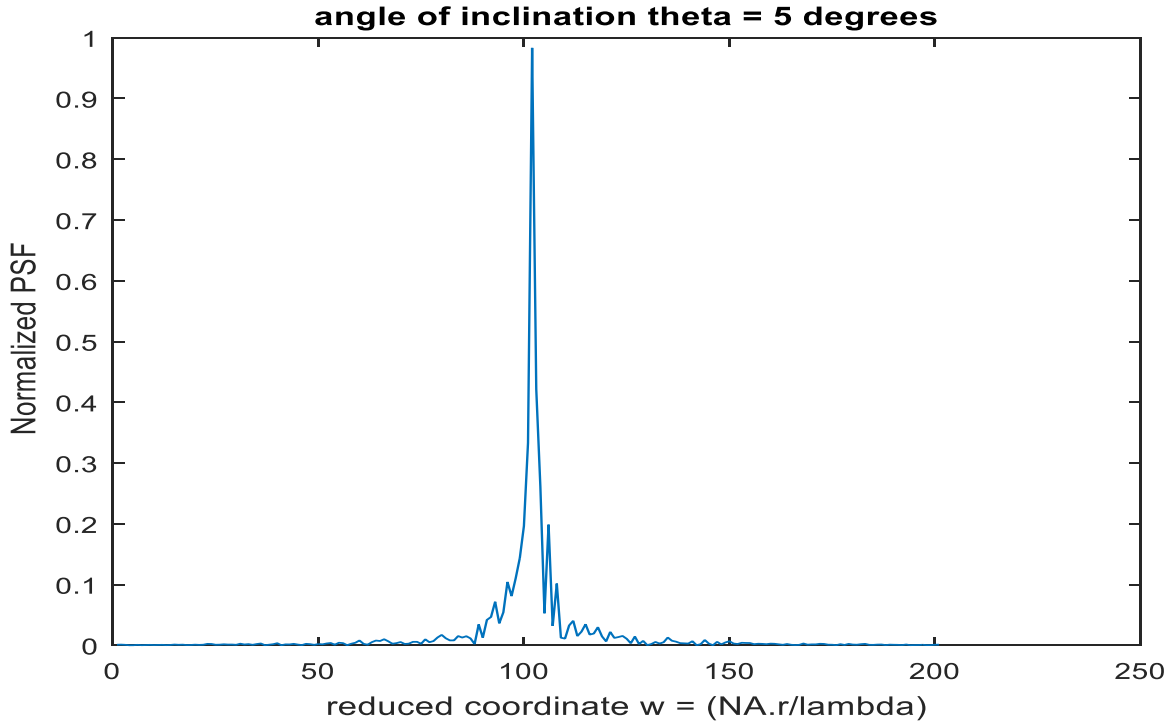

Figure 5- a: The normalized PSF for the inclined cardiac image at an angle $\theta = 5^0$.

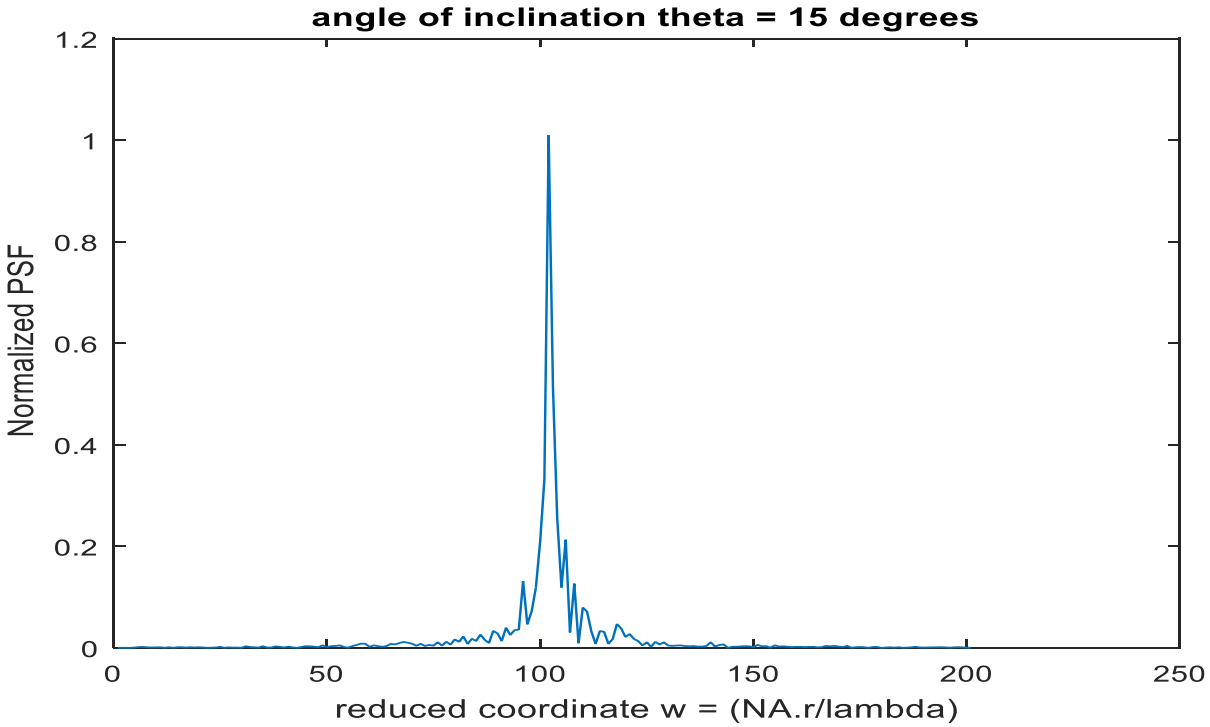

Figure 5- b: The normalized PSF for the inclined cardiac image at an angle $\theta = 15^0$.

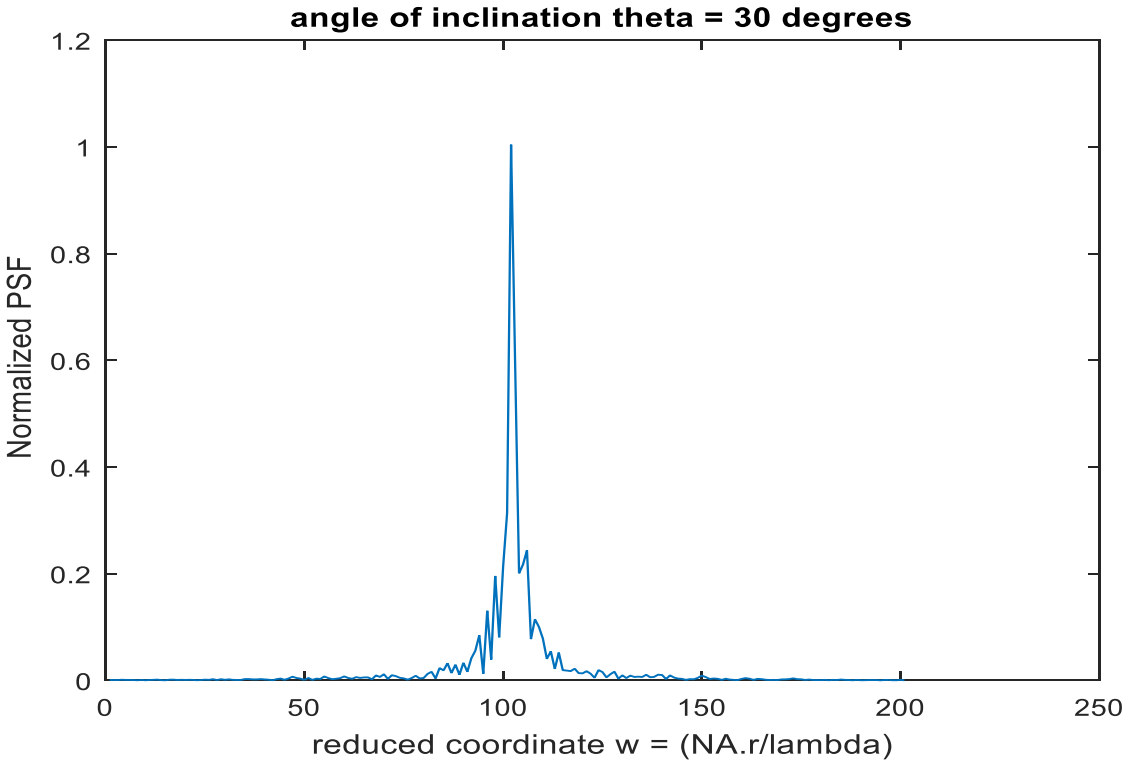

Figure 5- c: The normalized PSF for the inclined cardiac image at an angle $\theta = 30^0$.

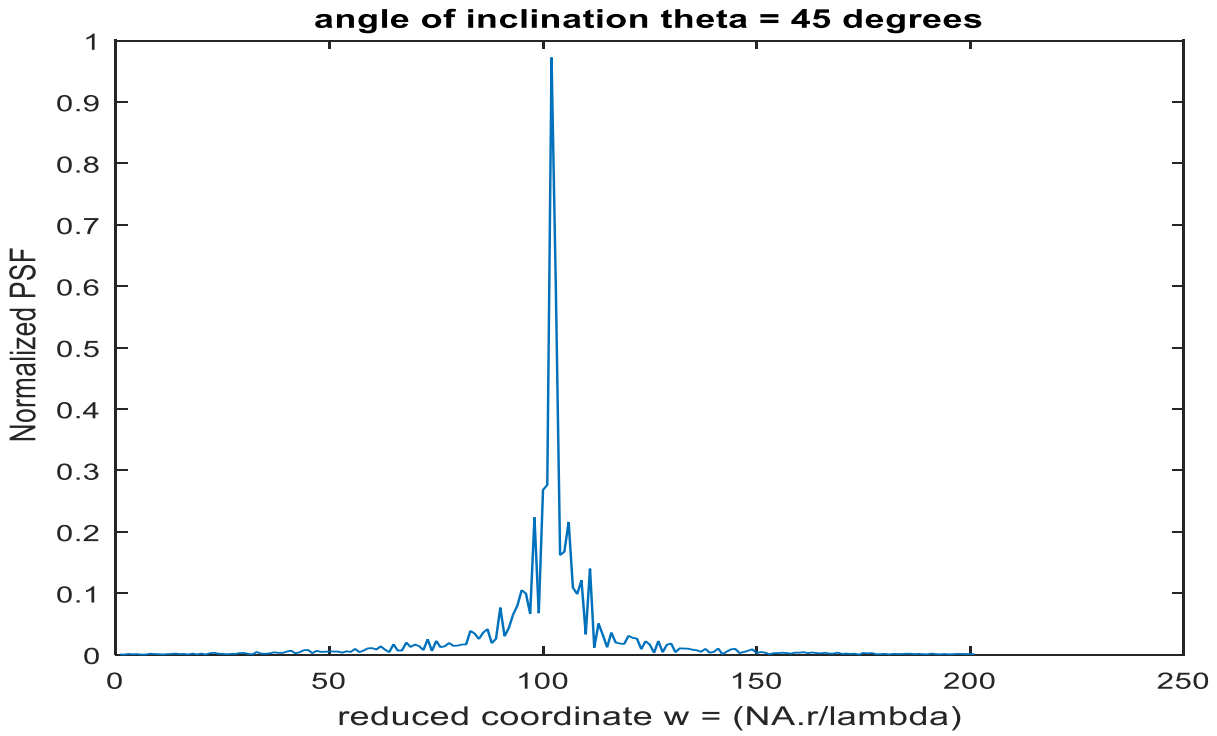

Figure 5- d: The normalized PSF for the inclined cardiac image at an angle $\theta = 45^0$.

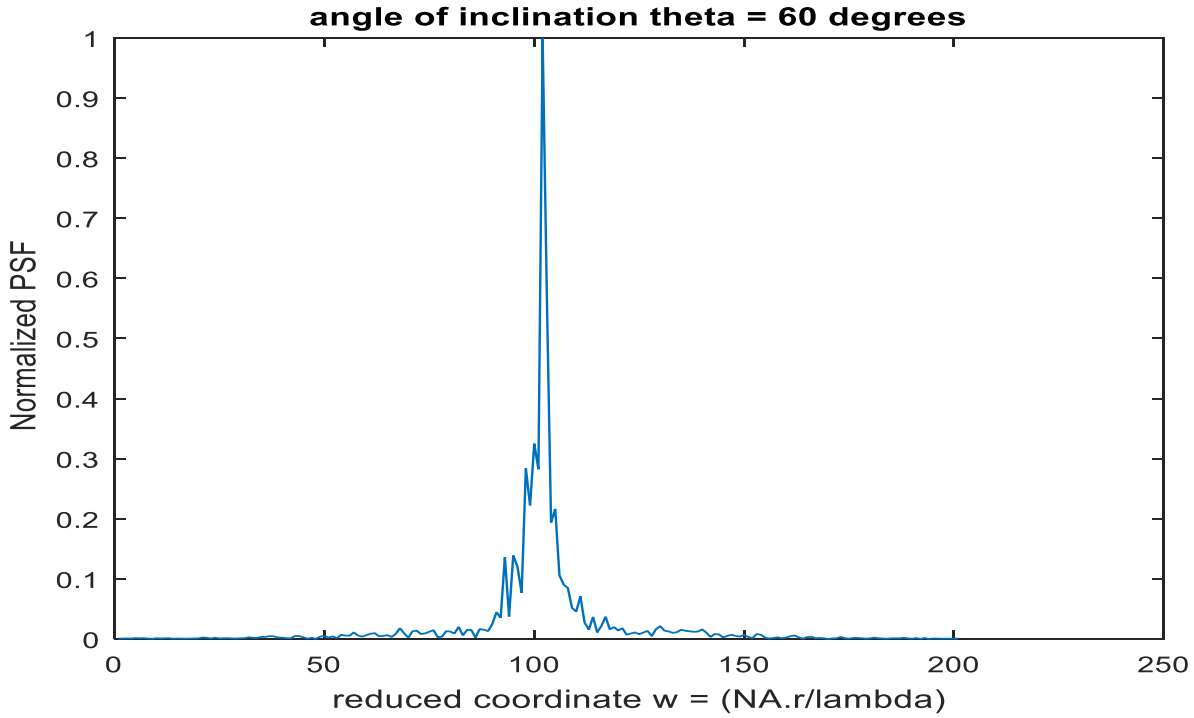

Figure 5- e: The normalized PSF for the inclined cardiac image at an angle $\theta = 60^0$.

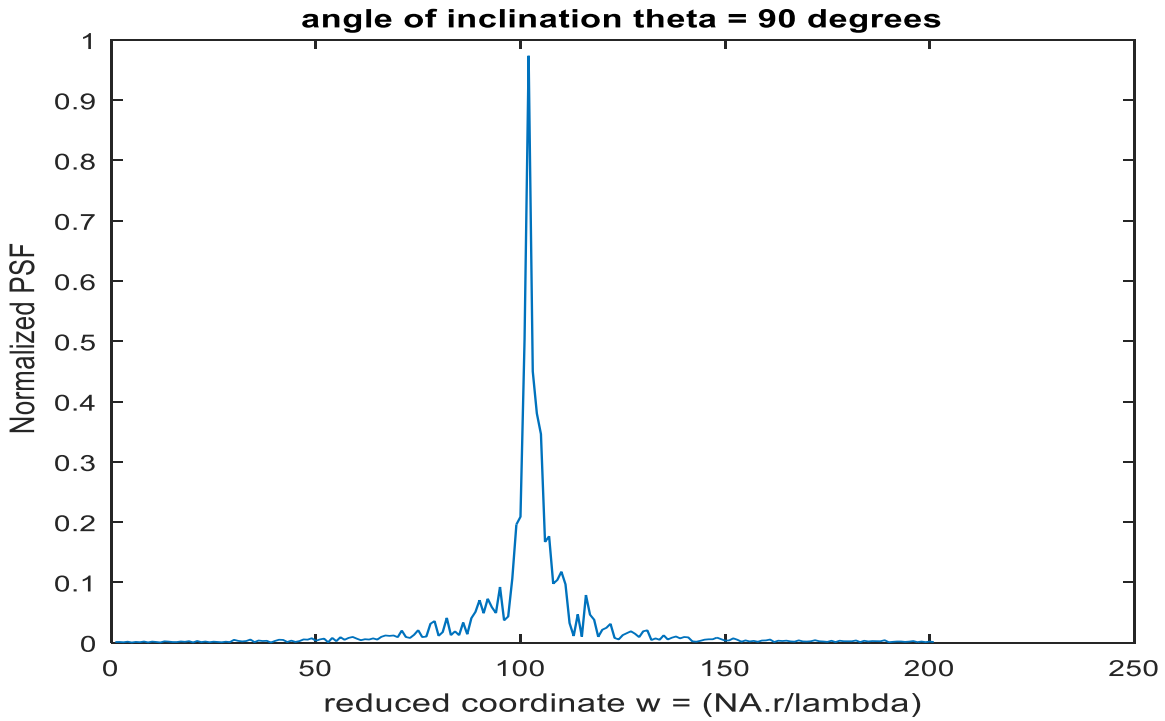

Figure 5- f: The normalized PSF for the inclined cardiac image at an angle $\theta = 90^0$.

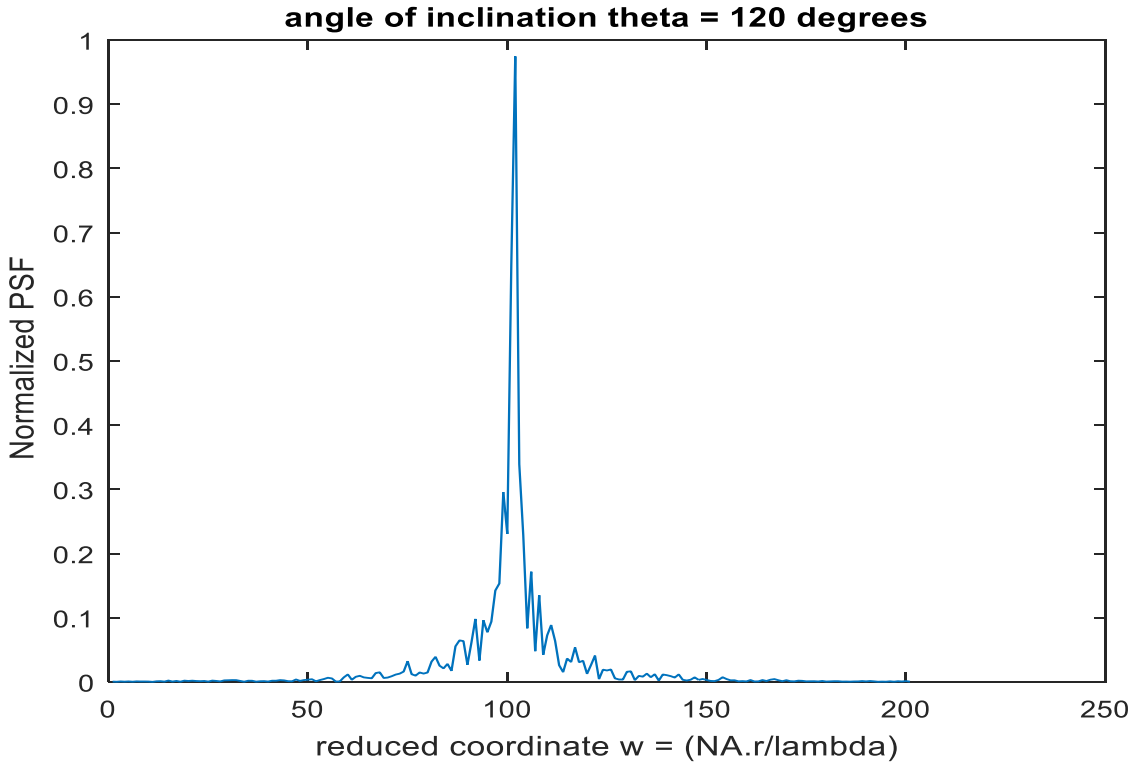

Figure 5- g: The normalized PSF for the inclined cardiac image at an angle $\theta = 120^0$.

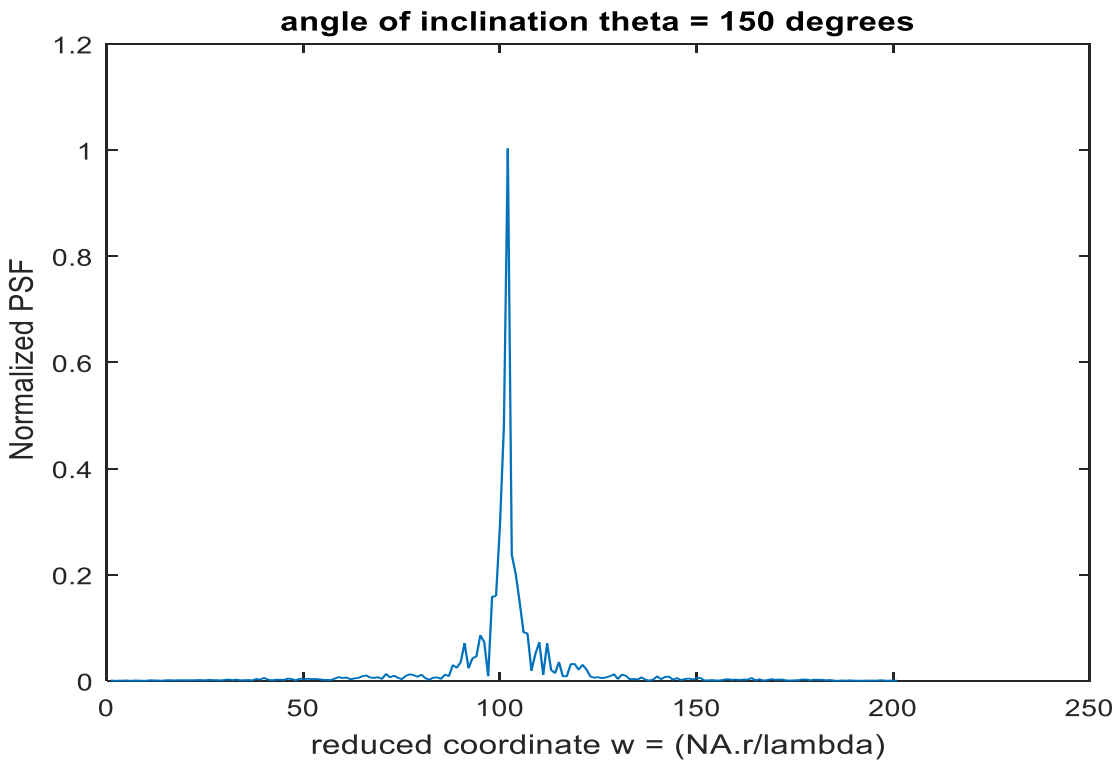

Figure 5- h: The normalized PSF for the inclined cardiac image at an angle $\theta = 150^0$.

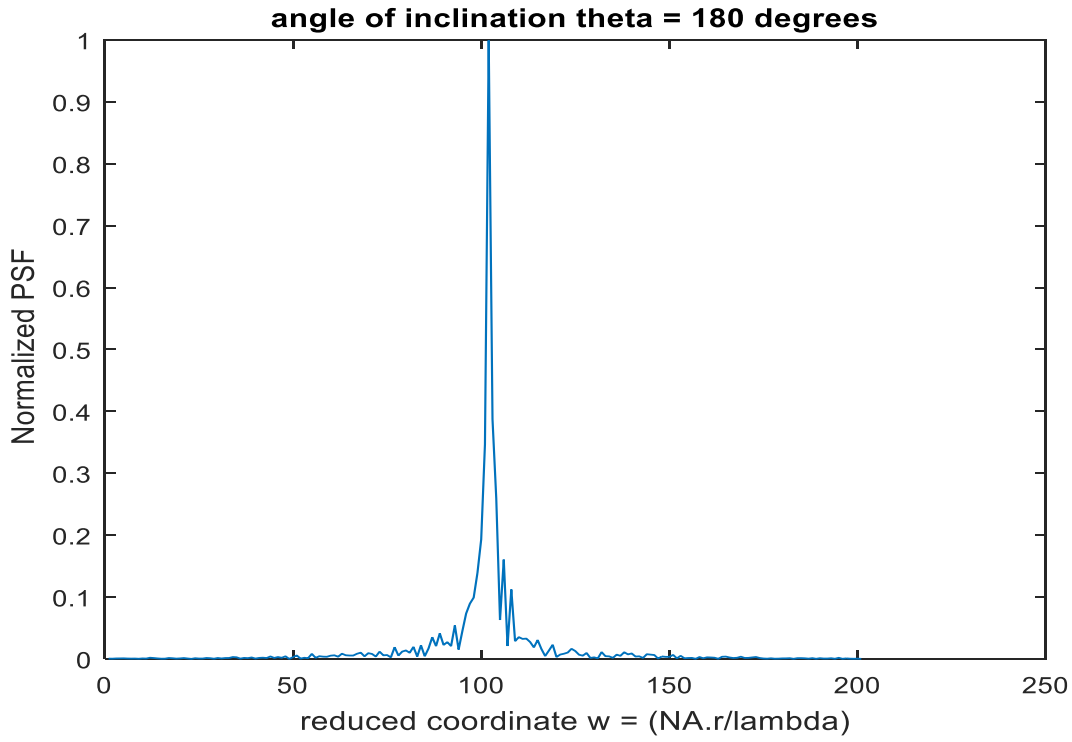

Figure 5- i: The normalized PSF for the inclined cardiac image at an angle $\theta = 180^0$.

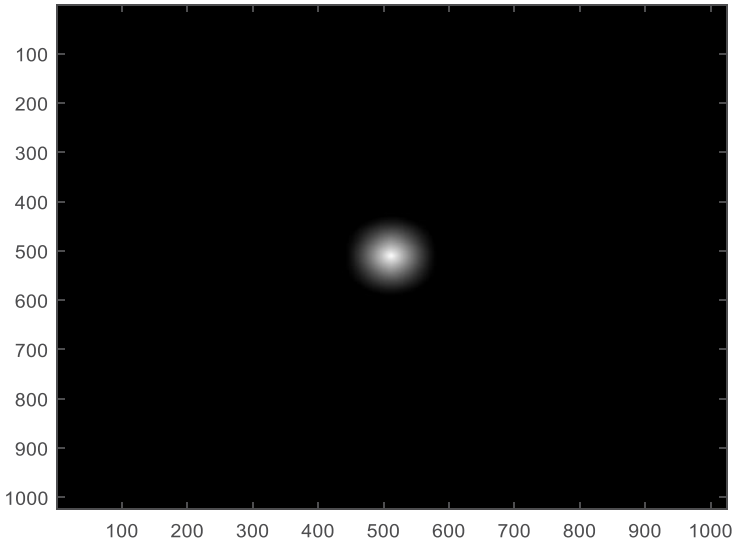

Figure 6: Autocorrelation of the aperture of the cardioid shape shown in Figure (2).

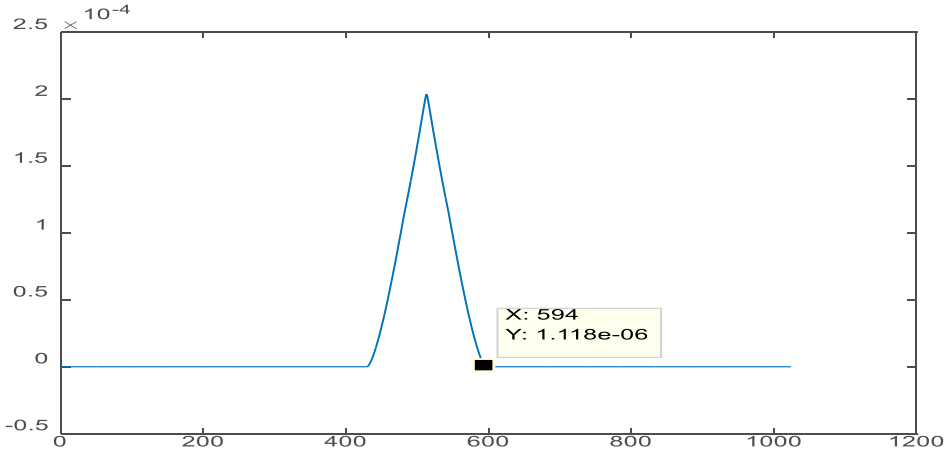

Figure 7- a: Line plot corresponding to the autocorrelation of the cardioid model at y = 512 pixels. The FWHM = 81 pixels

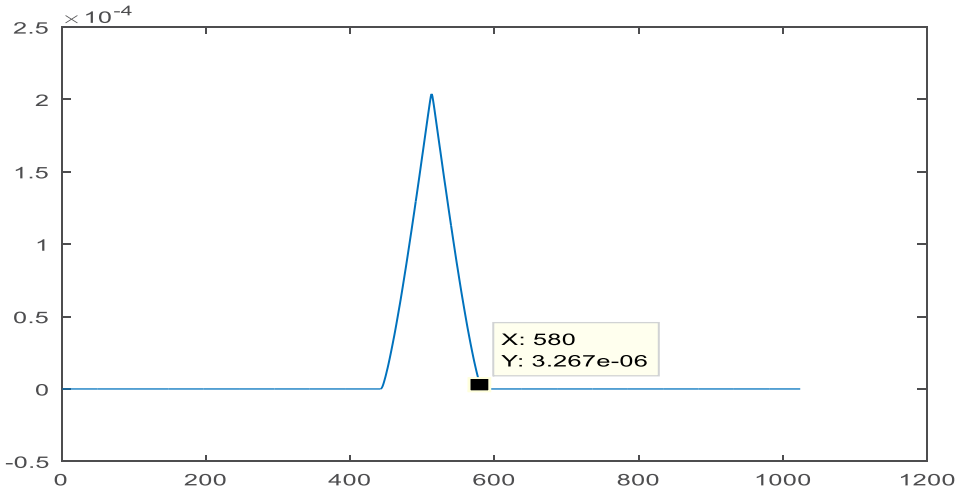

Figure 7- b: Line plot corresponding to the autocorrelation of the cardioid model at x = 512 pixels. The FWHM = 68 pixels.

The autocorrelation intensity of the heart image is shown in Figure (8). It shows a luminous spot at the center surrounded by a blurred image as expected from the geometry of the heart image with its arteries. The line plot corresponds to the autocorrelation of heart at x= 512 pixels shown in figure (9-a) and the corresponding FWHM = 307 pixels While the autocorrelation at y = 512 pixels shown in figure (9-b) and the corresponding FWHM = 403 pixels. It shows irregular distribution originating from the shape of the heat image in both plots. The cross-correlation of aligned and rotated cardiac images computed and plotted, for angles of rotations θ = 30, 60, and 900, as shown in figure (10- a). while cross-correlations plots, for angles of rotations θ = 120, 150, and 180 deg., are shown in figure (10- b). It shows different shapes for cross-correlation depending on the angle of rotation. It shows an asymmetric shape compared with the symmetric autocorrelation of the aligned cardiac image. The Cardiac and circular apertures used in the formation of images in the confocal microscope are shown in Figure (11-a). The maximum radius for the cardiac aperture equals the circular radius = 64 pixels. The original cardiac image and its reconstructed image using cardiac and circular apertures are shown in Figure (11-a) plotted in Figure (11-b) while using two symmetric circular apertures shown in Figure (11-c). All images have the same matrix dimensions of 512× 512 pixels.

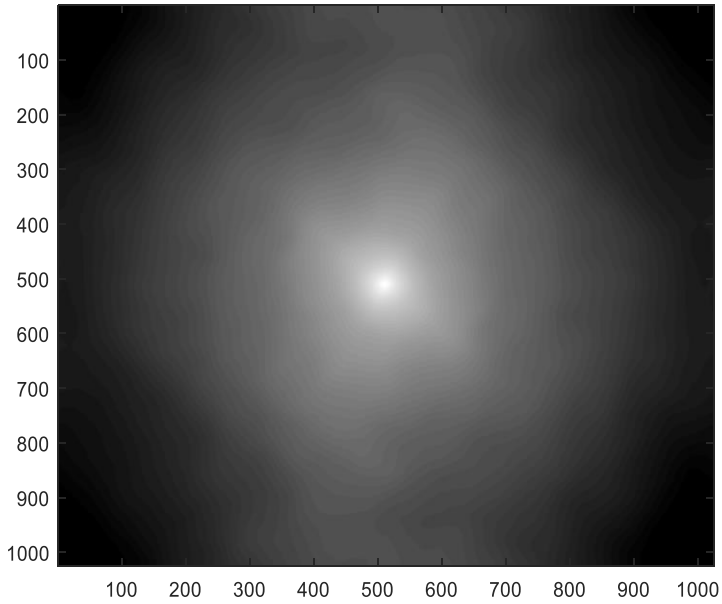

Figure 8: Autocorrelation intensity of heart image shown in figure (1).

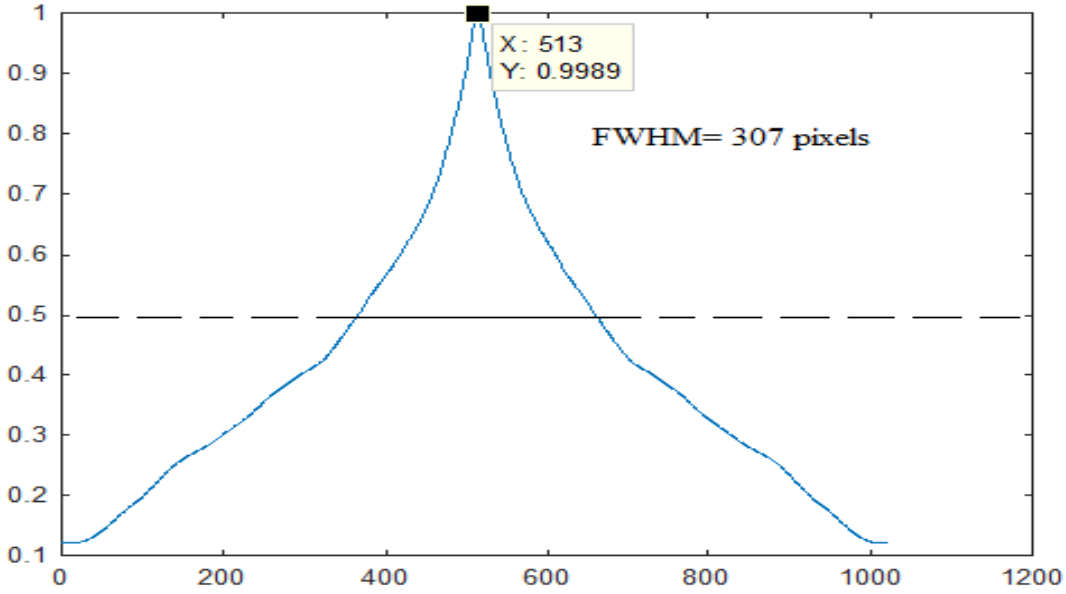

Figure 9- a: Line plot corresponding to the autocorrelation of heart at x= 512 px.

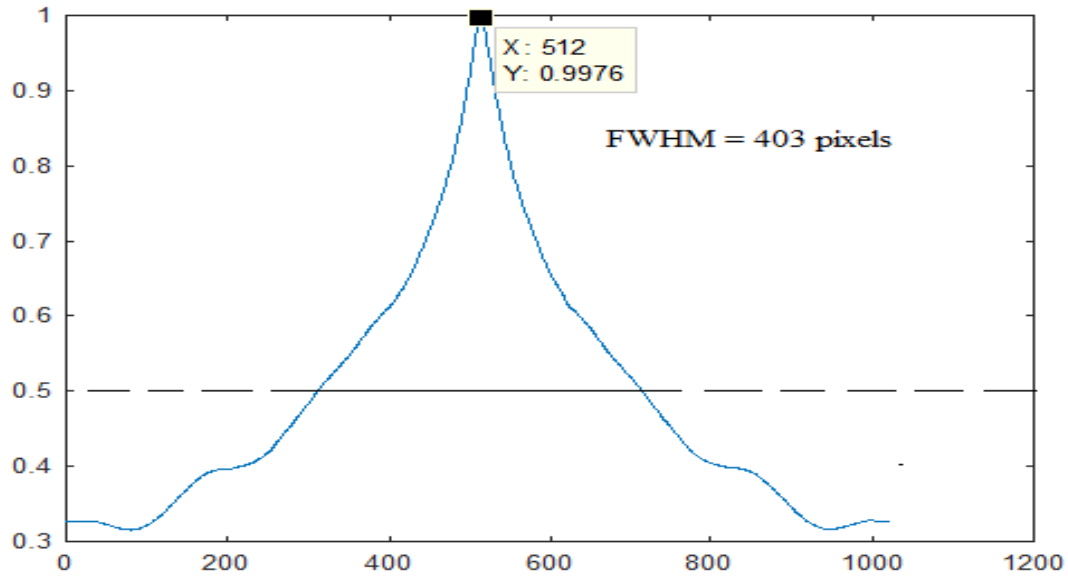

Figure 9- b: Line plot corresponding to the autocorrelation of heart at y = 512 px.

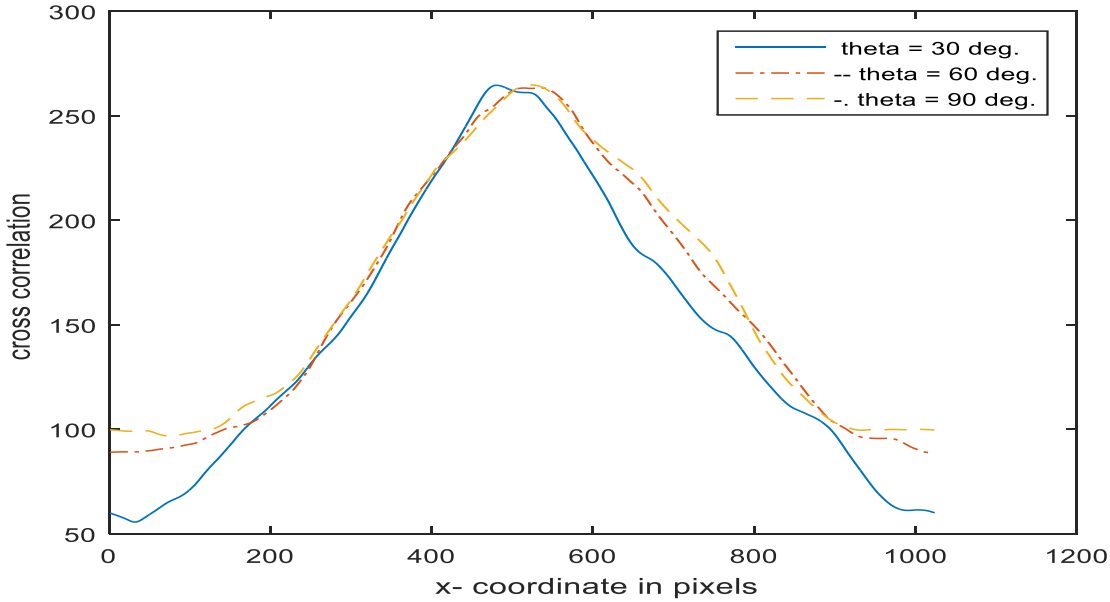

Figure 10- a: Cross-correlation corresponding to the unrotated heart image and the rotated images at angles of 30, 60, and 900.

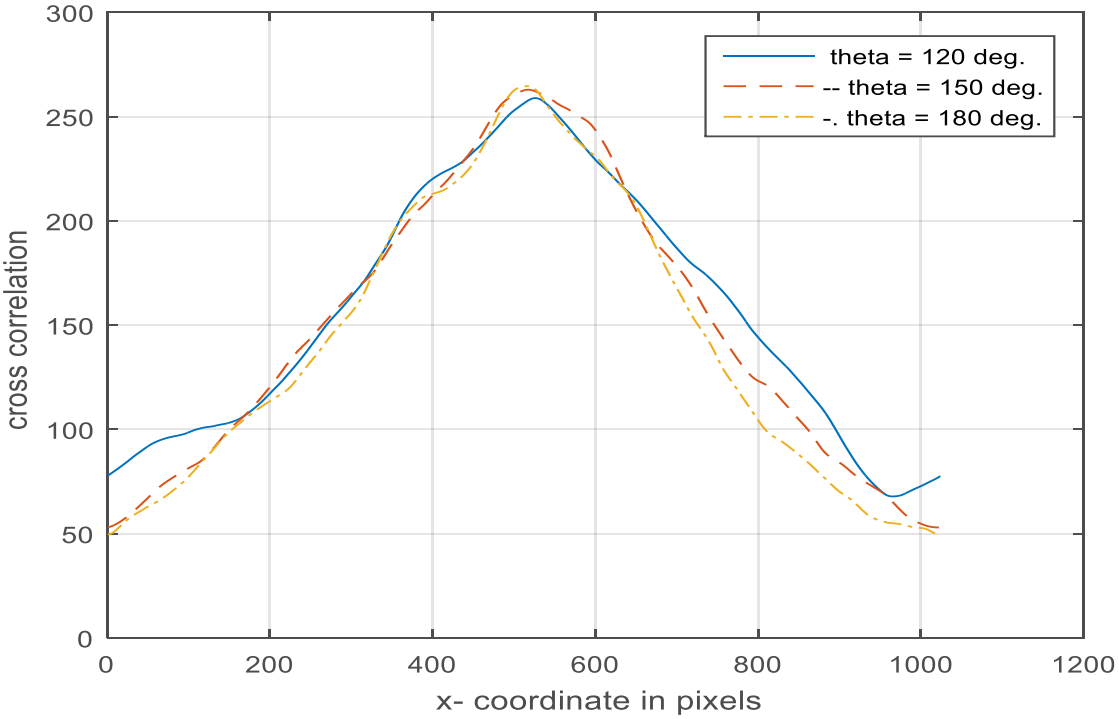

Figure 10- b: Cross-correlation at angles of 120, 150, and 180^0.

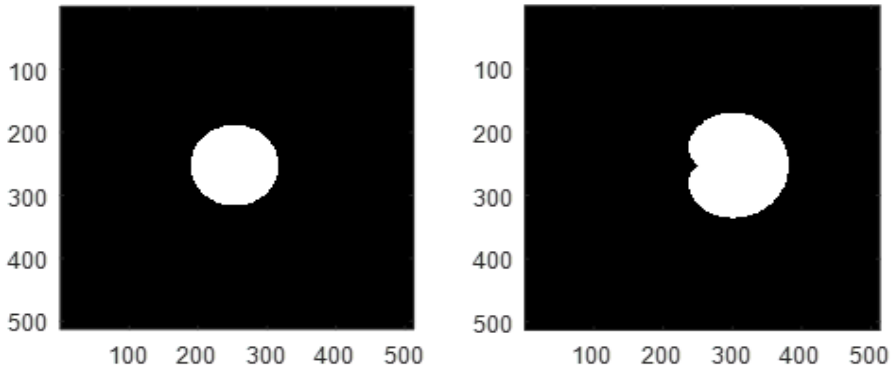

Figure 11- a: Apertures used in the formation of images using the confocal microscope.

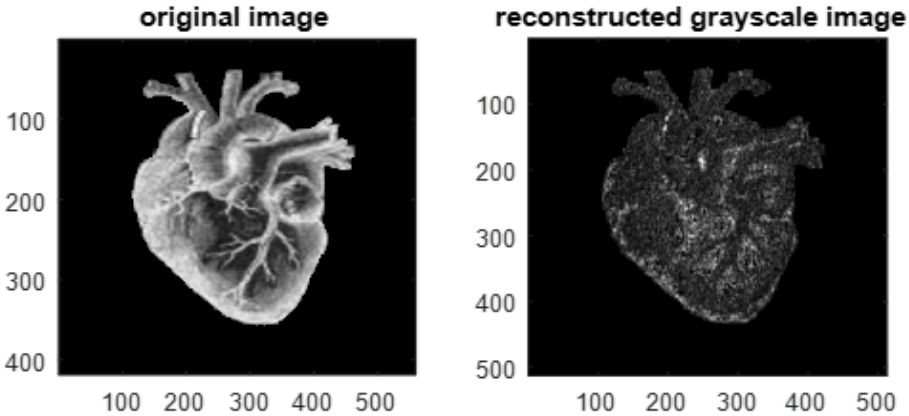

Figure 11- b: The original cardiac image and its reconstructed image. The images have the same matrix dimensions of 512× 512 pixels. Cardiac and circular apertures shown in Figure (11- a) were used for the reconstruction using the confocal microscope.

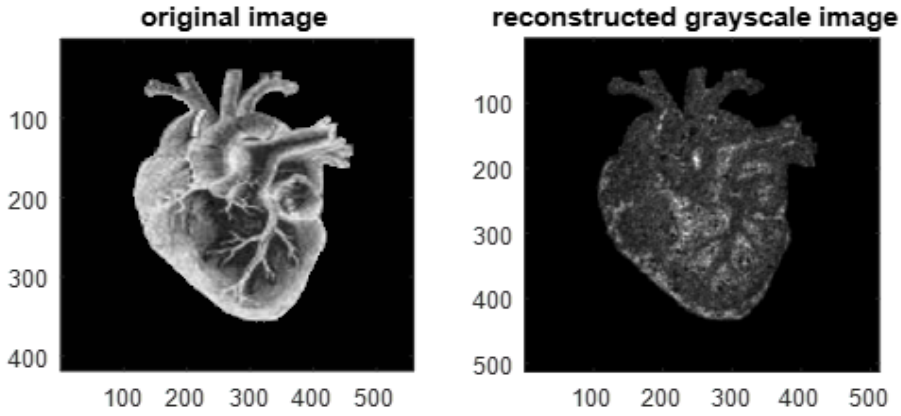

Figure 11- c: The original cardiac image and its reconstructed image. The images have the same matrix dimensions of 512× 512 pixels. Circular apertures are used for the reconstruction using the confocal microscope.

4. Conclusions

Firstly, the heart image is compared with the aperture of the geometric cardioid. It shows PSF symmetric shape in the case of the aperture as compared with the asymmetric curve in the case of the heart image. The FWHM computed from the PSF for the heart image is narrower than the corresponding one for the cardioid model and circular apertures. In addition, the heart image rotation showed different PSF profiles in the range ≤ 0.3 around the peak of different irregularities.

Secondly, the aperture of the cardioid shape has a narrower FWHM = 15 pixels compared with the FWHM= 20 pixels for the circular aperture considering the same radius at 32 pixels. Hence, we showed that the cardioid aperture may provide better results than the conventional circular aperture when used in a confocal set-up. Thirdly, the autocorrelation corresponding to the heart image along the cartesian coordinates showed different values for the FWHM. It is attributed to the different dimensions due to image elongation. In addition, it has irregular symmetric distribution depending on the image shape. While the comparative cardioid aperture showed a triangular shape. The cross-correlation of the aligned and rotated cardiac images showed irregular asymmetric distribution.
Finally, the reconstructed images obtained using a confocal microscope showed moderately resolved images dependent on the PSF for the cardioid aperture as compared with the PSF corresponding to the ordinary circular apertures.

5. Declaration

Ethics Approval: Not applicable.

Competing Interests: The authors declare that they have no competing interests.

Funding: Not applicable.

Availability of Data and Material: No Data associated with the manuscript.

References

1. Refael, CG. and Woods, RE. (2001). Digital Image Processing, Prentice Hall, Upper Saddle River, New Jersey 07458, 2nd Edition.
2. SEMMLO, J. L. (2004). Biosignal and biomedical image processing.
3. Jähne, Bernd (2002). Digital image processing, Springer Berlin, 5th edition.
4. Aho, A. V., & Hopcroft, J. E. (1974). The design and analysis of computer algorithms. Pearson Education India.
5. Arce, G.R., Gallagher, N.C., and Nodes, T.A. (1986). Median filters: theory for one- and two-dimensional filters, JAI Press, Greenwich, USA.
6. Dougherty, E. R. (1999). Random processes for image and signal processing. (No Title).
7. Kerre, E. E., & Nachtegael, M. (Eds.). (2000). Fuzzy techniques in image processing (Vol. 52). Springer Science & Business Media.
8. Hamed, A.M. (2009). Numerical speckle images formed by diffusers using modulated conical and linear apertures. Journal of Modern Opt. 56, 10, 1174.
9. Hamed, A.M. (2009). Formation of speckle images formed for diffusers illuminated by modulated apertures (circular obstruction) Journal of Modern Opt. 56, 15, 1633.
10. Hamed, A.M. (2011). Discrimination between speckle images using diffusers modulated by some deformed apertures: simulation. Optical Engineering 50, 1, 018202.
11. Hamed, A. M. (2020). Image processing of Ramses II statue using speckle photography modulated by a new Hamming linear aperture. Pramana, 94(1), 126.
12. Hamed, A. M. (2021). Contrast of laser speckle images using some modulated apertures. Pramana, 95(3), 122.
13. Hamed, A.M. and Al-Saeed, T. (2015). Image analysis of modified Hamming aperture: application on confocal microscopy and holography. J. Modern Opt. 62, 10, 801.
14. Hamed, A.M. (2017). Improvement of point spread function (PSF) using linear quadratic aperture. Optik, 131, 838.
15. Hamed, A. M., & Al-Saeed, T. (2023). Reconstruction of cardiac images using the confocal microscopy.

16. Pégard, N. C., Liu, H. Y., Antipa, N., Gerlock, M., Adesnik, H., & Waller, L. (2016). Compressive light-field microscopy for 3D neural activity recording. Optica, 3(5), 517-524.
17. Seidel, T., Edelman, J.C., and Sachse, F.B. (2016). Analyzing Remodeling of Cardiac Tissue: A Comprehensive Approach Based on Confocal Microscopy and 3D Reconstruction. Annals of Biomedical Engineering, 44, 5, 1436.
18. Huang, C., Wasmund, S., Hitchcock, R., Marrouche, N. F., & Sachse, F. B. (2017). Catheterized fiber-optics confocal microscopy of the beating heart in situ. Circulation: Cardiovascular Imaging, 10(10), e006881.